Research Square

Preprints are preliminary reports that have not undergone peer review.
They should not be considered conclusive, used to inform clinical practice,
or referenced by the media as validated information.

Performance Prediction of Geocell-Reinforced Foundation Beds Using Artificial Neural Networks

Mohammad Javad Hosseinzadeh
Tarbiat Modares University
Mohammad Oliaei
M.olyaei@modares.ac.ir

Tarbiat Modares University
Saeed Kouzegaran
University of Mazandaran

Article

Keywords: Geosynthetics, Geocell, Numerical Analysis, Bearing Capacity Ratio, Artificial Neural Networks

Posted Date: November 23rd, 2026

DOI: https://doi.org/10.21203/rs.3.rs-11674252/v1

License: This work is licensed under a Creative Commons Attribution 4.0 International License.
Read Full License

Additional Declarations: No competing interests reported.

PERFORMANCE PREDICTION OF GEOCELL-REINFORCED FOUNDATION BEDS USING ARTIFICIAL NEURAL NETWORKS

Authors

Mohammad Javad Hosseinzadeh [a], Mohammad Oliaei* [b], Saeed Kouzegaran [c]

a Department of Civil Engineering, Tarbiat Modares University, Tehran, Iran. Hosseinzadeh.m@modares.ac.ir

b Supervisor, Department of Civil Engineering, Tarbiat Modares University, Tehran, Iran. M.olyaei@modares.ac.ir. Room 6-609, Faculty of Civil and Environmental Eng., Tarbiat Modares University, TEHRAN, IRAN. +982182884395.

c Advisor, Faculty of Technology and Engineering, University of Mazandaran, Babolsar, Iran. Skouzegaran@umz.ac.ir

Abstract

Predicting the performance of geocell-reinforced foundations is essential, but difficult, as current experimental and numerical approaches struggle with the complex nonlinear nature of these systems. In this study, an Artificial Neural Network (ANN) was developed to predict the Bearing Capacity (BC) and the Bearing Capacity Ratio (BCR) of geocell-reinforced foundation beds in comparison with unreinforced samples. An extensive database, including 1574 samples, was created through 3-D Finite Element Method (FEM) analyses. The numerical model was initially validated by comparing its results with those from published experimental studies. It was then utilized to explore a wide variety of soil conditions, geocell properties, and geometries. Afterwards, a multilayer perceptron with three hidden layers was generated and trained using the stress-settlement curves and derived bearing capacity values from the numerical FEM analyses. The BC models achieved average test R^2 of 0.986 and 0.914 for the unreinforced and reinforced datasets. A second model predicting BCR directly to isolate the reinforcement benefit from the soil-dominated baseline achieved an R^2 of 0.883. Shapley Additive exPlanations (SHAP) analysis showed soil-strength parameters (cohesion, friction angle, elastic modulus) govern absolute bearing capacity, while the BCR model revealed that the reinforcement benefit depends primarily on the baseline soil condition and is enhanced by geocell stiffness and geometry. The proposed

ANN model presents an efficient alternative to time-consuming and expensive finite element analyses, which can be used for preliminary assessment and design processes for geocell-reinforced foundation systems.

Keywords

Geosynthetics, Geocell, Numerical Analysis, Bearing Capacity Ratio, Artificial Neural Networks

1. Introduction

The growth of population and construction activity has reduced the availability of good construction sites in urban areas, whereas many regions, such as coastal and seashore zones, are underlain by inherently weak or problematic soils. Consequently, the need for in-situ improvement of weak soil beneath most structures, especially shallow foundations, is increasing significantly. Rather than relying on conventional deep foundations, such as pile-supported systems, engineers are increasingly adopting geosynthetic-reinforced soil (GRS) technology, which is a cost-effective and environmentally friendly alternative. Over the past three decades, extensive experimental and numerical studies have confirmed that such reinforced systems provide high performance and excellent load-bearing capacity, while offering long-term durability, non-corrosiveness, resistance to chemical and biological degradation, lightness, ease of installation, and rapid construction. Soil reinforcement is therefore among the most popular ground-improvement techniques, and geosynthetic-reinforced soil has attracted considerable attention from engineers and researchers as an efficient means of enhancing foundation performance.

Among the various geosynthetics, planar geogrid reinforcement has been one of the most accessible methods and has been studied since the 1980s [1]. Geogrid reinforcement in soil foundations has been proven to increase the bearing capacity and reduce settlement [2-7]. Accordingly, several studies have provided such analyses and presented formulations to predict the bearing capacity of reinforced foundations [8-11].

The demand for higher confinement from reinforcement has led to advances in geocell-reinforced soils. Geocells, like most other geosynthetic materials, are made of polymeric materials; however, their three-dimensional honeycomb geometry provides a confinement mechanism that distinguishes them from other planar geosynthetics. Comparative tests on geocells and planar geotextiles have shown that, for the same amount of material, geocells strengthen the soil more noticeably and reduce settlement more effectively under practical footing loads [12,13]. Dash et al. [14] illustrated that geocell confinement promotes more effective load redistribution over a wider soil area than planar or unreinforced conditions. Geocell reinforcement has also proven beneficial for road embankments [15-17], circular footings [18,19], railroads [20], foundation beds [21] and plate anchors under uplift [22,23]. Collectively, these studies reported benefits such as greater cohesive strength, smaller permanent deformations, reduced vertical stress, and diminished settlements [20].

Several researchers have conducted experimental tests on geocell-reinforced soil and demonstrated that reinforcement reliably enhances soil stiffness and strength by improving lateral confinement, with performance being strongly influenced by factors such as geocell geometry, material stiffness, infill density, and confining pressure [4,24-27]. Square-footing plate-load tests on coir geocell–reinforced sand have likewise reported a bearing-capacity ratio of about 2.65 at a settlement of 10% of the footing width under both concentric and eccentric load [28]. Despite reliable results, experimental research methods are time-consuming and design calculations often require quick analyses to understand the impact of different parameters.

In addition to experimental investigations, numerical modelling has been widely used to analyze geosynthetic-reinforced foundation systems, so that many more configurations can be explored for the same time and money. Some earlier studies replaced geocell confinement and interfacial resistance with a stiffer layer of soil with equivalent strength and stiffness, which lacks realism by disregarding parametric uncertainties despite simplifying the model. Although this composite approach shows reasonable agreement with experimental observations, it is often restricted to case-specific conditions and lacks general applicability, limiting its ability to explicitly capture soil-reinforcement interaction mechanisms in various cases. To overcome these shortcomings, more refined investigations have explicitly modelled geocell reinforcement as single- or multi-cell systems, allowing for a realistic representation of confinement and stress transfer [29]. Hegde and Sitharam [30] modelled the actual curved geometry of a geocell mattress as a multiple-cell system. Zhao et al. used the same three-dimensional cell geometry in FLAC3D for cohesive beds with different infills, checking the model against plate-load tests; a high-modulus, low-cohesion infill gave the largest improvement [31]. Three-dimensional simulations of reinforced sand and soft-soil foundations have also confirmed that geocells can significantly increase the bearing capacity and reduce settlement [32-36].

Although numerical and analytical methods provide valuable insights and behavioral details, they are computationally expensive and time-consuming, and most are limited to specific soil types, reinforcement geometries, or loading conditions. To address these limitations, artificial intelligence techniques, including artificial neural networks, machine learning, and deep learning, have been increasingly adopted to predict foundation performance, and geosynthetic-reinforced soil systems are not excluded from this trend. Neural networks trained on finite-element campaigns have been used to classify the stability of unreinforced footings on two-layer soil [37], and SHAP values with partial dependence plots have been used to interpret laboratory bearing-capacity models for granular soils [38]. For geogrid reinforcement, researchers have coupled ANNs with optimization algorithms, such as gray wolf optimization, to predict the response of GRS foundations and Harris hawk optimization to predict the settlement of geosynthetic-reinforced soil abutments, outperforming several conventional machine learning models [39,40]. Kumar et al. [41] further examined the optimal placement depth of geogrid and geocell reinforcement and predicted bearing capacity ratios using combined experimental and ANN approaches.

For geocell-reinforced soil specifically, Saride et al.[42] developed multiple-regression and ANN prediction models and stressed the importance of diverse training datasets, while Kumar and Kumar[43] used a back-propagation neural network to predict raft settlement on geocell-reinforced sand from variables such as relative density, reinforcement depth, and geocell layer number and height. More recent studies have applied genetic programming, multivariate adaptive regression splines, and multilayer perceptrons to geocell systems, identifying the most influential parameters and the effects of pocket size and infill modulus on improvement factors [44,45]. Feng et al. trained a voting ensemble, interpreted with SHAP, to predict the failure mode of geocell-reinforced footings from two-dimensional particle-flow simulations; geocell height, relative density and load

eccentricity dominated [46]. That study does not predict bearing capacity or the bearing-capacity ratio, and it does not use a three-dimensional continuum model of the honeycomb. Nevertheless, most prior geocell-ANN studies report accuracy without interpreting which variables drive reinforcement benefits relative to baseline capacity, and studies focusing on improvement ratios remain narrow in scope.

Although these intelligent techniques are state-of-the-art, they are generally case-specific and trained on relatively small experimental datasets covering particular soils, footing configurations, or geocell geometries, which limits their generalizability. A comprehensive model that estimates the bearing capacity of geocell-reinforced foundation beds from large-scale numerical parametric simulations is therefore still required. The present study addresses this gap by predicting the bearing capacity of unreinforced and geocell-reinforced foundations and measuring the benefits of the reinforcement. First, a three-dimensional finite element model was generated in ABAQUS and validated against the experimental results of Hegde and Sitharam [30]. Once the model was validated, it was used to build a large numerical database with varying soil conditions and geocell properties across 1574 analyses. Two separate ANN models were developed using this data; one predicting the absolute bearing capacity and the other targeting the bearing capacity ratio, which isolates the benefit of the geocell from the soil's own strength. SHAP values ranked the inputs and guided a backward elimination of the least useful features, and partial dependence plots traced how each parameter affected the prediction.

2. Methodology

This section focuses on the numerical analysis in the ABAQUS software and the development of the neural network model using Python. The numerical simulation consists of two steps: first, the primary model is explained and validated based on the literature, and then the main numerical model of the foundation beds is investigated. Subsequently, the process of developing the neural network model is described in different steps, and tools for interpreting the outcomes are clarified.

2.1 Numerical Analysis

2.1.1 Initial Numerical Model

Validating numerical models against reliable experimental data is essential to ensure the accuracy and reliability of computational simulations in geotechnical engineering. In this study, the experimental and numerical investigations conducted by Hegde and Sitharam[30] were used to validate the proposed numerical model. In their experimental test, a cast-iron tank with dimensions of 900 mm × 900 mm and a height of 600 mm was used. The tank was fitted to a loading frame, and the load was applied through a square-shaped steel plate. Sandy soil with a specific gravity of 2.64 and a friction angle of 36° was used in the test, which is classified as poorly graded (SP) according to the Unified Soil Classification System. The schematic layout of the test setup is illustrated in Fig. 1, and the properties of the reinforcement materials are listed in Table 1.

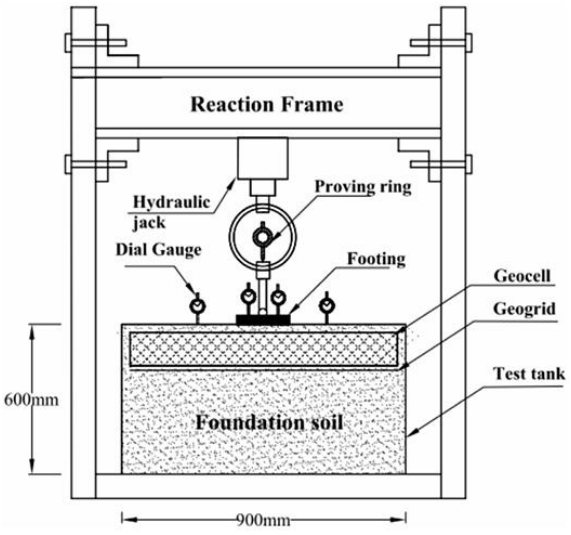

Fig. 1 Schematic view of the experimental test setup[30]

Table 1 Reinforcement properties[30]

Parameters	Quantity
Geocell	
Polymer	Polyethylene
Cell size (mm)	250 × 210
No. of cells/m2	40
Cell depth (mm)	150
Strip thickness (mm)	1.53
Cell seam strength (N)	2150 (±5%)
Density (g/cm3)	0.95 (±1.5%)
Short-term yield strength (kN/m)	20
Geogrid	
Polymer	Polypropylene
Aperture size (mm)	35 × 35
Ultimate tensile strength (kN/m)	20
Mass per unit area (g/m2)	220
Shape of aperture opening	Square

A 3D numerical model was created in ABAQUS based on the experimental setup. To simulate the soil behavior, the Mohr-Coulomb constitutive model was used with key parameters, including unit weight, elastic modulus, Poisson's ratio, friction angle, dilation angle, and cohesion. Furthermore, the geocells were modeled as a linear elastic plastic material. All relevant material properties for the soil and the reinforcement were adopted from the study of Hegde and Sitharam[30], as summarized in Table 2.

Table 2 Material properties used for the numerical analysis[30]

Parameters	Values
Sand	
Shear modulus, G (MPa)	5.77
Bulk modulus, K (MPa)	12.5
Poisson's ratio, υ	0.3
Friction angle, φ (°)	36
Unit weight, γ (kN/m3)	20
Geocells	
Young's modulus, E (MPa)	275
Poisson's ratio, μ	0.45
Thickness, t_i (mm)	1.5

Due to the symmetry of the test setup, only one quarter of the test bed was simulated to optimize computational efficiency. To simulate the test tank conditions, lateral movement was restrained on the two vertical sides of the soil block in the x- and z-directions, and a symmetry condition was applied to the two other sides. The bottom boundary was fixed against movement in all directions. The analysis was performed in two steps: first, applying the gravity loads, and then applying the external loading. The loading area was a 75 mm × 75 mm square, and the load was applied under displacement-controlled conditions up to 30 mm. The soil was meshed using hexahedral eight-noded elements (C3D8R) in both models. The geocell in the reinforced model was modeled as a continuous sheet with a height of 150 mm, following the actual curved pocket geometry with 250 × 210 mm openings, and meshed with four noded membrane elements (M3D4R).

2.1.2 Model Validation

The numerical results showed good agreement with both the experimental and numerical results reported by Hegde and Sitharam[30], as illustrated in Fig. 2 where S shows the settlement and B is the foundation width. After the model was validated, it was used for the subsequent analyses of the foundation beds of this study with minor adjustments to the simulation process.

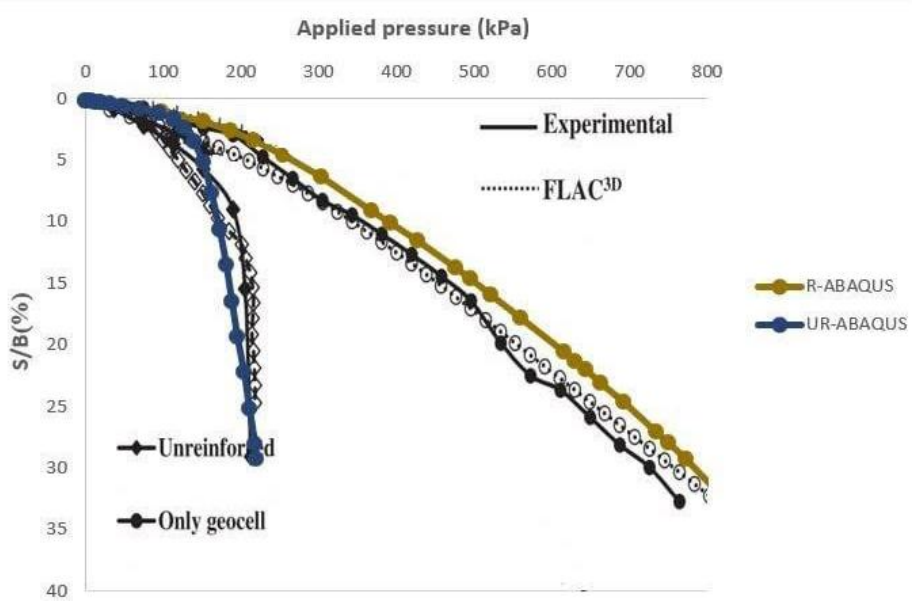

Fig. 2 Comparison of numerical analysis results with work of Hegde and Sitharam[30]

2.1.3 Main Numerical Model

Based on the validated model, a baseline numerical model was developed to investigate the behavior of geocell-reinforced foundations. A parametric study was conducted to evaluate the influence of various soil and geocell parameters on the foundation's bearing capacity. The soil block was 500 × 500 mm with a height of 500 mm, though these dimensions were modified when multi-layer reinforcement was used.

- **Soil Database and Parameter Selection**

To establish a comprehensive and realistic dataset for predicting the bearing capacity of geocell-reinforced foundations, soil parameters were extracted from a wide range of reputable geotechnical engineering textbooks and academic literature. This extensive multi-source compilation ensures that the selected parameter ranges cover a broad spectrum of realistic engineering properties. This process yielded a total of 623 soil samples, which incorporate both synthesized parameter ranges and collected data from existing studies to ensure dataset diversity. Table 3 shows the data ranges extracted from reference books.

Table 3 Soil parameters selected from reference books

Soil Name	Dry Unit Weight (kN/m^3)	Elasticity Modulus (MPa)	Friction Angle	Cohesion (kPa)	Total Tests
Loose uniform sand	14-16	10-30	29-35	-	27
Medium Sand	16-18	25-55	30-39	-	48
Dense uniform sand	18-20	50-80	36-45	-	48
Loose angular-grained silty sand	13-16	5-15	20-26	-	36
Dense angular-grained silty sand	17-20	20-30	29-35	-	36
Soft clay	12-14	5-25	18-24	20-40	81
Medium Clay	14-16	20-40	21-27	50-70	81
Stiff clay	16-18	50-90	27-33	80-110	180
Total Number of Tests (soil's strength parameters)					537

After running the analysis for a total of 623 samples in both unreinforced and reinforced conditions, a parametric study was conducted to evaluate the influence of geocell properties and geometric configurations including the following parameters: geocell modulus (E_g), number of layers (N), embedment depth to foundation width ratio (Df/B), height to foundation width ratio (h/B), opening diameter to height ratio (d/h), and geocell layer width to foundation width ratio (b/B). Additionally, two additional loading area dimensions were analyzed beyond the primary dimensions. The details of all these parameters are presented in Table 4. When investigating the effect of each reinforcement or geometry parameter, eight soil samples were used, each representing one of the eight groups of soil. The specifications of these eight soil samples are listed in Table 5, and a summary of all datasets is provided in Table 6.

Table 4 Reinforcement and geometrical parameters of the non-soil parameter analyses

Parameter	Values	Total Tests
Geocell Modulus	55, 165, 275, 825, 1375	64
No. of Layers	1, 2, 3	32
D_f/B	0, 0.25, 0.5, 0.75, 1	80
h/B	0.5, 0.75, 1, 1.25, 1.5	64
d/h	1.33, 1.67, 2	16
b/B	1, 2, 3, 4	40
Loading Area	100 * 100 100 * 200 150 * 250	32

Table 5 Soil parameters of the eight representative soil samples selected for reinforced soil analysis

No.	Soil Type	Density (kN/m³)	E (MPa)	Poisson's Ratio	φ (°)	c (kPa)
1	Loose sand	15	20	0.3	30	10
2	Medium sand	17	40	0.3	36	10
3	Dense sand	19	70	0.35	42	10
4	Loose silty sand	14	10	0.3	22	10
5	Dense silty sand	18	30	0.3	32	10
6	Soft clay	13	15	0.2	20	30
7	Medium clay	15	30	0.3	24	60
8	Stiff clay	17	70	0.35	30	90

Table 6 Overview of the numerical simulation runs

	Unreinforced	Reinforced	Total Tests
Soil Parameters based on Reference Books	537	537	1074
Soil Parameters from the Literature	86	86	172
Geocell Parameters	4	292	296
Geometrical Parameters	16	16	32
Sum	643	931	1574

- **Geometrical Conditions**

The boundary conditions were the same as those of the validation model. The two sides were allowed to move only in the vertical direction, while symmetry boundary conditions were applied to the remaining two sides. In the reinforced model, the geocell was embedded at depths corresponding to the Df/B ratios presented in Table 4. The analysis steps and load magnitude, were kept the same as those in the evaluation model of Hegde and Sitharam, while the loading area was changed to 100 × 100 mm, as shown in Fig. 3. To investigate the effect of the loading area, its dimensions were varied to represent different foundation geometries.

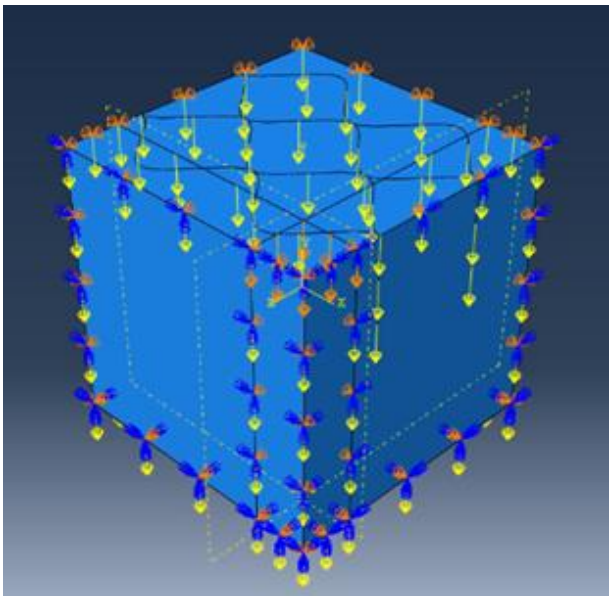

Fig. 3 Loading and boundary conditions

- **Meshing Conditions**

The part instance for the soil block was meshed by seeding generally and specifically on the edges of the block. Finer mesh was considered for the loading area for more precision. Using hexahedral eight-noded elements (C3D8R), the soil block was discretized into 4096 elements for both unreinforced and reinforced conditions. The geocell was modelled using 1024 four-noded membrane elements. The number of elements differed when the height of the geocell layer was modified. A mesh sensitivity study was performed to ensure that further mesh refinement produced negligible changes in the predicted settlement and stress values.

2.2 Neural Network Model

Artificial neural networks (ANNs) are a tool in the wide range of machine learning algorithms capable of predicting system behavior based on available data. The idea is inspired by the behavior of the human nervous system and was first proposed by McCulloch and Pitts in 1943. The structure of a simple ANN involves three layers, namely the input layer where data enters, the hidden layer(s) where it is processed, and the output layer. These layers consist of interconnected processing units, known as neurons (or nodes), which interact through weighted connections. Fig. 4 shows a typical structure of an ANN proposed by Goh in 1995[47].

The model is trained to learn the correlations between the input parameters, assess their effect on the outcome, and minimize the error between measured outputs and predicted ones by adjusting weights and biases. In this study, the network's parameters were optimized using the

backpropagation algorithm as well as the Adam optimizer. During training, a loss function (e.g., Mean Squared Error) is minimized by sequentially introducing input-output patterns and updating weights from the output to the input layer.

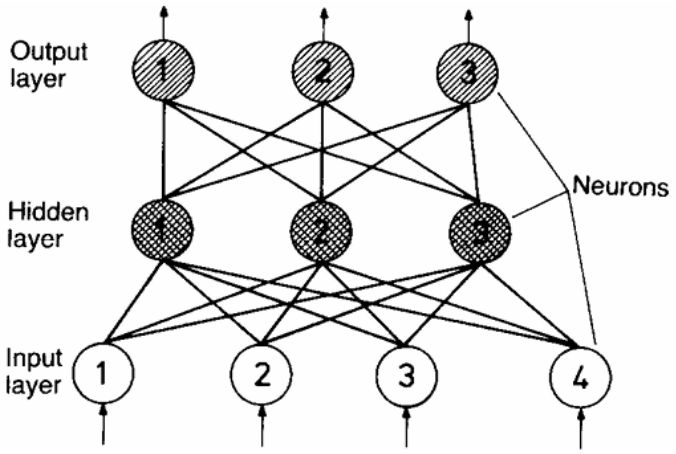

Fig. 4 Typical neural network architecture by Goh (1995)

The performance of the ANNs was evaluated using various standard metrics, such as the coefficient of determination (R^2), Root Mean Square Error (RMSE), and Mean Absolute Error (MAE). These network models are widely used for different engineering purposes because they can build empirical correlations between input and output variables without requiring prior assumptions. Consequently, researchers can extract relevant and even complex information from training datasets and solve complex problems and nonlinear fitting models with higher accuracy and certainty.

2.2.1 Data Preparation, Parameter Selection, and Model Architecture

The numerical analysis produced two outputs: stress on the loading area (in kPa) and settlement (in mm). These outputs were obtained for 1574 different samples, and stress-settlement curves were generated for all samples. The data was then preprocessed for the neural network using Python in the Jupyter Notebook environment. At this stage, all curves were carefully examined, and the bearing capacity was derived from each stress–settlement curve using a consistent criterion applied uniformly to all cases, resulting in a clean dataset. Moreover, the data were checked, and duplicate samples were removed. The dataset was then divided into two sets based on reinforcement condition, since geocell parameters do not affect the results of unreinforced samples. The reinforced model trains only on reinforced samples with non-zero geocell parameters, whereas the unreinforced model was trained on soil-only inputs. However, the loading area (A) was included in both datasets.

Feature selection is an important step that can improve the performance and generalization of the model. Its advantages include the elimination of redundant parameters, reduced training time, and improved prediction accuracy. In this study, features were selected based on their engineering relevance; a SHAP (SHapley Additive exPlanations)-based elimination procedure was then used to confirm that all retained variables contributed independently to the prediction. Based on these methods, cohesion (c), friction angle (φ), elastic modulus (E_s), unit weight (γ), and Poisson's ratio (ν) were selected from soil parameters. From the geocell parameters, elastic modulus (E_g), number of layers (N), embedment depth to foundation width ratio (D_f/B), height to foundation width ratio (h/B), geocell width to foundation width ratio (b/B), and opening diameter to height ratio (d/h) were selected. Together with the loading area (A), these resulted in 12 input features for the reinforced model and 6 input features for the unreinforced model (which excludes the geocell-related parameters). These input parameters were common to both predictive models developed in this study; the target variables (bearing capacity and bearing capacity ratio) are defined in the respective model subsections.

Before training, all input and output variables were standardized using the StandardScaler function, which ensured that they contributed equally during training. Standardization parameters were computed from the training set only and applied to the validation and testing subsets to avoid information leakage. The dataset was randomly divided into training, validation, and testing segments, with portions of 60%, 20%, and 20%, respectively. Each subset was used for different purposes. The network weights were updated using the training set in a batch size of 32, and the validation set was used for hyperparameter tuning and early stopping. The testing set was used to assess the model's performance and accuracy. In addition to this three-part division, a five-fold cross-validation was performed to examine the generalization and robustness of the model. In each fold, data standardization was performed independently using statistics of the corresponding training partition.

Using TensorFlow/Keras, a feedforward multilayer perceptron (MLP) was developed as the common predictive architecture for both models. The network comprises an input layer, three hidden layers, and an output layer. The number of neurons in the input layer depended on the dataset, with 6 and 12 input variables considered for the unreinforced and reinforced models, respectively. The hidden layers consisted of 128, 64, and 32 neurons, and utilized the swish activation function. The He Normal was implemented to initialize the weights, as it selects them with a scaled normal distribution that improves stability and convergence later in training. A linear activation function was used in the output layer to predict the target values.

Overfitting and underfitting are two of the most common problems associated with neural networks. Therefore, several techniques were adopted to reduce their occurrence. In this study, several regularization methods were used to enhance generalization and reduce overfitting. After the first two hidden layers, batch normalization was used to stabilize the learning process and accelerate convergence. Additionally, dropout with different rates for each layer, L2 regularization, and MaxNorm weight constraint were applied to the necessary layers. Model parameters were

updated through backpropagation using the Adam optimization algorithm, with the mean absolute error (MAE) monitored as a supplementary metric. This architecture, data-handling, and training protocol were common to both models; different aspects such as target variable, loss function, and hyperparameter-selection strategy are described in the following subsections.

2.2.2 Bearing Capacity (BC) Model

The first developed model was focused mainly on predicting the absolute bearing capacity (BC) in kPa for two different unreinforced and reinforced datasets with 6 and 12 input variables, respectively. During training, the mean squared error (MSE) was adopted as the loss function, and early stopping was applied when the validation loss did not improve over 300 consecutive epochs. Training was conducted for different numbers of epochs, and 2000 epochs were found to be sufficient, as further training led to negligible improvement in the performance metrics. Additionally, if the validation loss flattened out for 100 epochs, the learning rate was reduced by a factor of 0.5 times from an initial value of 0.0001. The hyperparameters of this model were tuned by a manual trial-and-error procedure to find the best accuracy and prevent the model from overfitting. For this model, dropout rates of 0.5, 0.4, 0.3, and an L2 regularization factor of 0.01 were applied. Each model was trained three times to reduce the impact of random initialization and partitioning, and the average metrics were reported.

2.2.3 Bearing Capacity Ratio (BCR) Model

Since absolute BC is mostly soil-dominated and the impact of reinforcement parameters may not be fully reflected in the BC model, a second model was developed to predict the bearing capacity ratio (BCR). BCR is defined as the ratio of bearing capacity in reinforced condition to that of the unreinforced obtained from paired numerical results for identical soil and foundation conditions. The input parameters for this model are the same as those in the reinforced dataset of the primary model, and the output is BCR. The unreinforced bearing capacity was excluded as an input, since it forms the denominator of the target and would otherwise introduce leakage. BCR values were right-skewed (skewness $\approx$ 1.4), so they were log-transformed before training and back-transformed for evaluation to stabilize variance.

The network architecture was kept the same as the primary model, while hyperparameters were tuned using a systematic grid search over 36 combinations of L2, dropout schedules, and learning rate values. Each combination was repeated over 3 seeds, forming 108 trials in total, and evaluated exclusively on the validation set, to reach the best combination with L2 = 0.01, dropout = 0.4/0.3/0.2, learning rate = 0.002. The final predictions were averaged over five independently trained networks, with per-seed mean ± standard deviation reported alongside the ensemble result. Optimized hyperparameters were used for this final version, and Huber loss was implemented instead of MSE as a more robust loss function for the high-BCR tail.

2.3 Model Interpretation

Even though neural networks can predict outputs with high accuracy, they have a black-box nature, and their interpretability should be improved. SHAP (Lundberg and Lee, 2017) were used in the current paper to quantify the contribution of each input parameter to the predicted output parameter of each model. In this study, SHAP values were computed using the Deep Explainer, which is exact for the feed-forward network, and were evaluated over the full test set. The mean absolute SHAP value of each parameter was calculated and then used to generate a ranking of feature importance.

Furthermore, a summary plot was created to illustrate the magnitude and direction of each parameter's impact on the output of our model. In addition to the raw mean SHAP rankings, a normalized (range-weighted) importance was computed, where the mean absolute SHAP value of each feature was weighted by its sampled range, so that the importance of a variable is not conflated with the width of its sampled interval. Moreover, SHAP dependence plots were produced for all of the parameters, with discussions mainly focused on the primary and most influential parameters in more detail. Permutation importance analysis was also performed to verify the reliability of SHAP-based rankings.

3. Results and Discussion

This study consists of two major parts: numerical analysis and a neural network prediction model. In the first part, a reliable dataset consisting of 1574 stress-settlement curves was generated through three-dimensional finite element analyses of reinforced and unreinforced foundations. Bearing capacities were extracted from the generated stress–settlement curves, and the corresponding BCR values were subsequently calculated. In this section, the generated numerical datasets are first examined regarding bearing capacity outcomes, parameter ranges, and statistical properties. In the second part, an ANN was developed, trained, validated, and tested using the unreinforced and reinforced datasets, and different metrics and interpretation tools were employed to assess and explain their performance.

3.1 Numerical Analysis Results

In this section, the results from numerical analysis of geocell-reinforced foundations are discussed. First, the behavior of the system and its stress-settlement curves are illustrated. After that, the statistics of input variables and their correlations are shown in detail, helping to demonstrate the versatility of the dataset and its initial correlations. Finally, the bearing capacity values extracted from the curves, their distribution, and the statistics of the calculated BCR values are discussed.

3.1.1 System Response and Stress-Settlement Behavior

The results from the three-dimensional finite element analyses provide a comprehensive view of the geocell-reinforced foundation behavior. The nonlinear response of the system is clearly illustrated in the stress-settlement curves (Fig. 5), where typical curves for sand, silty sand, and clay are presented. The inclusion of geocell reinforcement led to a consistent increase in stiffness and ultimate bearing capacity across all soil types. Weaker soil samples exhibited greater settlement susceptibility at identical stress levels, resulting in flatter stress-settlement curves and lower stiffness compared to denser sand or stiffer clays. The close agreement between these numerical results and published experimental data, as established in the validation study, confirms that the generated database is sufficiently accurate for training the ANN models.

The ranges covered by the input variables are presented in Tables 7 and 8 for the unreinforced and reinforced datasets, respectively. The coefficient of variation mentioned for each feature indicates the variability of each parameter relative to the mean and shows that most parameters exhibit high variability in this study. The large coefficient of variation for some geocell parameters, particularly Df/B, is primarily a consequence of the dataset construction. Since the majority of reinforced simulations adopted a baseline configuration with D_f/B of zero, and only a limited number of cases

considered embedded geocells, the parameter distribution is highly skewed, leading to an unusually high coefficient of variation.

The reliability of the generated database is supported by the validation study, in the previous sections, in which the numerical analysis of geocell-reinforced foundation showed close agreement with published experimental and numerical results. Therefore, the analyses conducted in this study were sufficiently accurate for generating the ANN dataset.

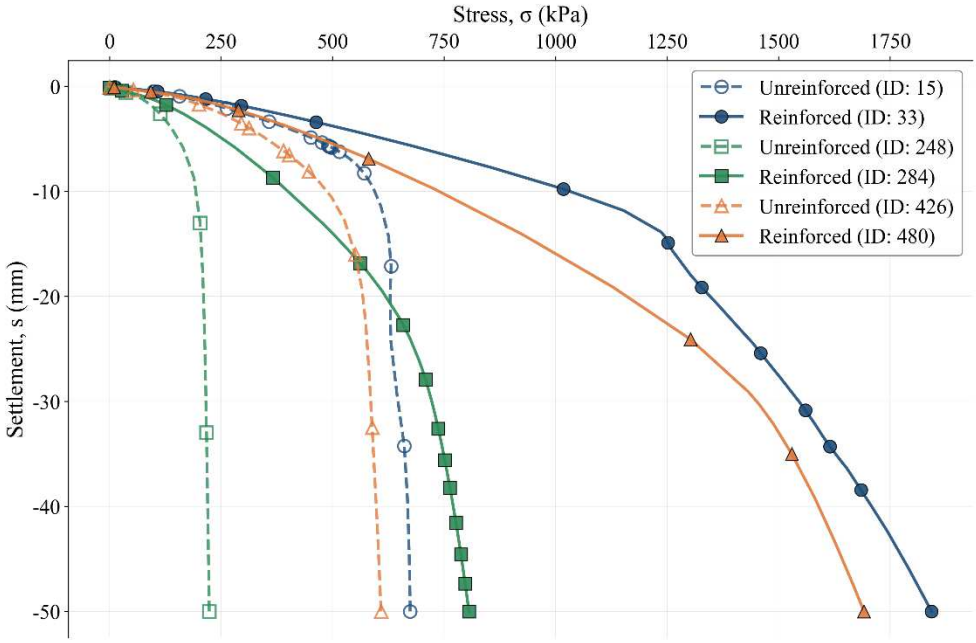

Fig. 5 Sample stress – settlement curves

Table 7 Statistical summary of the input variables (unreinforced)

Variable	Mean	Std	Min	Max	CV (%)
γ (kN/m³)	16.21	2.00	12	20.6	12.33
Es (MPa)	41.58	25.88	4.5	150	62.26
ν	0.306	0.048	0.2	0.42	15.57
φ (˚)	29.81	6.50	12	45	21.82
c (kPa)	43.07	37.13	1	110	86.21
A (m^2)	0.042	0.014	0.04	0.15	34.06
BC (kPa)	1683.4	1437.7	88.7	5742.1	85.4

Table 8 Statistical summary of the input variables (Reinforced)

Variable	Mean	Std	Min	Max	CV (%)
γ (kN/m³)	16.15	1.98	12	20.6	12.28
Es (MPa)	39.74	24.82	4.5	150	62.47
ν	0.304	0.046	0.2	0.42	15.26
φ (˚)	29.72	6.63	12	45	22.32
c (kPa)	38.64	35.31	1	110	91.38
Eg (MPa)	316.59	234.73	55	1375	74.14
Df/B	0.069	0.209	0	1	303.94
N	1.052	0.289	1	3	27.46
h/B	0.769	0.158	0.5	1.5	20.59
d/h	1.670	0.044	1.33	2	2.63
b/B	2.407	0.824	0.67	4	34.25
A (m^2)	0.047	0.024	0.04	0.15	51.18
BC (kPa)	2021.4	1652.4	208.1	8729.5	81.7

3.1.2 Simulation Statistics and Correlation Analysis

As shown in Table 6, a total of 1574 3-D numerical simulations were performed, with further details presented in Fig. 6. Most simulations were performed to determine the impact of soil parameters, with values extracted from reference books or the literature [48-56]. More than 296 analyses were allocated to the geocell parameters, whereas the geometrical parameters contributed the fewest runs. The relationships between the input parameters were examined using a correlation matrix, as shown in Fig. 7. Spearman correlation heatmap was generated which evaluates monotonic relationships based on rank order and is less sensitive to nonlinearity and outliers [57]. The results provide an initial assessment of the relationships among the parameters, showing that the elastic modulus has the strongest positive correlation with the output parameter, confirming the significant role of soil stiffness in governing the foundation response.

This dominance of soil parameters over reinforcement parameters in governing absolute bearing capacity motivates the development of a separate BCR model to isolate the reinforcement effect. In contrast, the weak linear correlations observed for most reinforcement parameters suggest more nonlinear and complex effects. These results highlight the need for machine learning approaches as more robust tools for investigating the nonlinear and interactive relationships between the parameters.

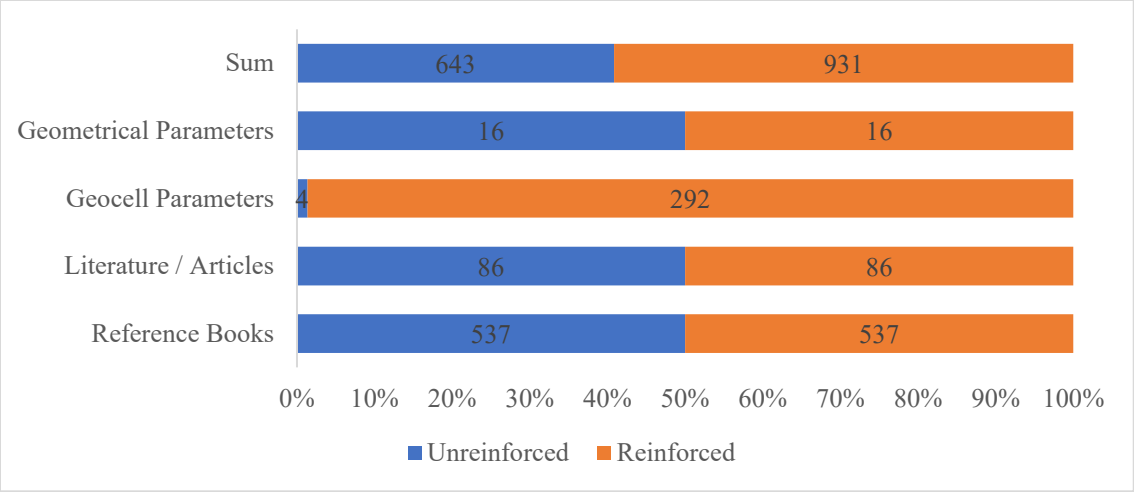

Fig. 6 Statistics of numerical simulations

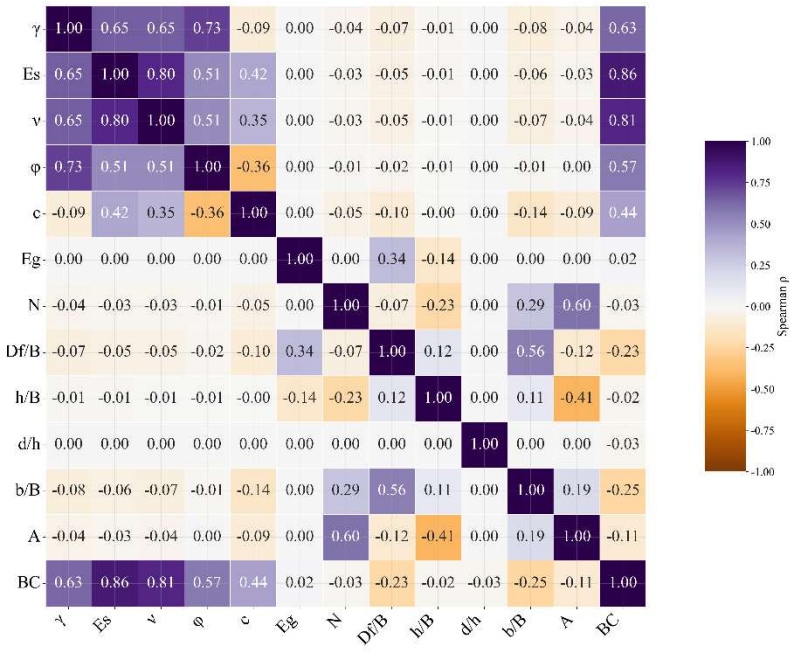

Fig. 7 Correlation matrix of the input features for the reinforced dataset

3.1.3 Bearing Capacity Distribution

The bearing capacities in the dataset used in this study covered a wide range of responses. Fig. 8 shows the distribution of bearing capacity values, together with the mean and median lines, providing a smoothed representation of the probability density. This figure confirms that the numerical simulations produced a broad range of foundation responses. The unreinforced dataset contained 643 samples with bearing capacities ranging from 88 to 5742 kPa, with an average of

1683 kPa, while the reinforced dataset consisted of 931 samples with bearing capacities from 208 to 8729 kPa, with an average of 2021 kPa. The higher mean, median, and upper-percentile values observed in the reinforced dataset demonstrate the beneficial influence of geocell reinforcement on foundation performance.

The coefficient of variation (CV) combined for both datasets was slightly higher than 83%, confirming the substantial variability of the dataset. The combined distribution presented moderate positive skewness (1.39) with a prevalence of low and intermediate bearing capacity values, and a smaller number of simulations with very high stress levels. Noticeable differences between the mean and median values in both datasets further confirm the positively skewed nature of the data. The dataset exhibited a relatively large interquartile range of 2301 kPa for unreinforced and 2028 for reinforced samples, demonstrating the broad range of soil and reinforcement conditions considered in this study. The cumulative distribution function (CDF), shown in Fig. 9, indicates a gradual increase across the entire range and confirms that the generated database includes a broad range of foundation responses, from poor bearing capacity conditions to heavily reinforced configurations. This diversity is highly beneficial for the training of our ANN model, since it reduces the risk of bias and improves model generalization.

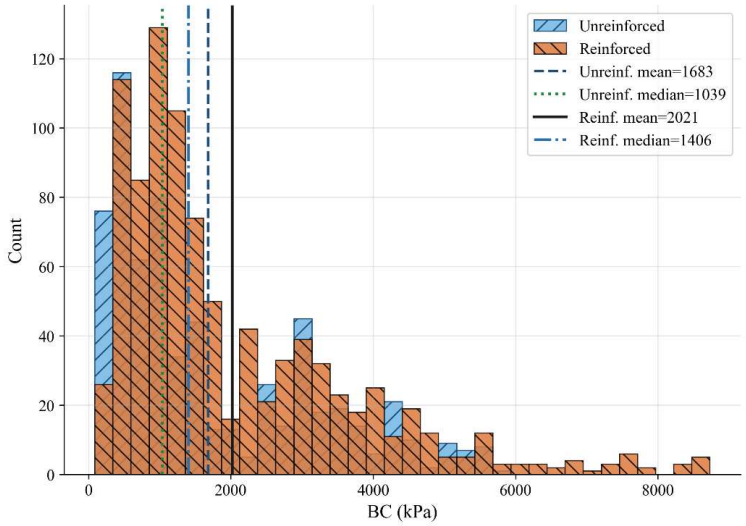

Fig. 8 Distribution of bearing capacity values

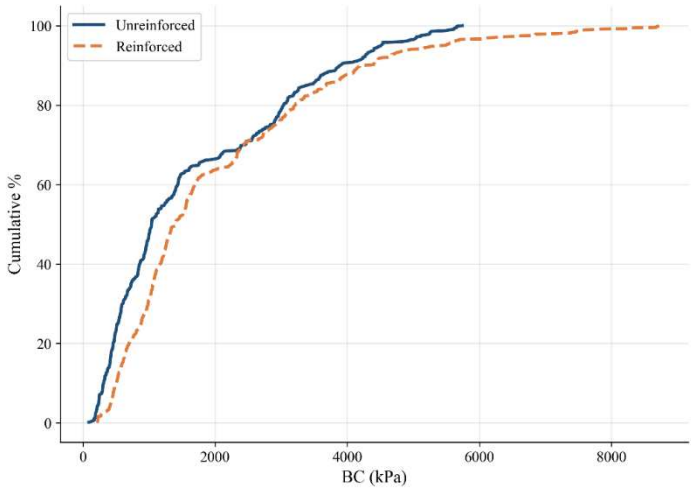

Fig. 9 Cumulative distribution function of bearing capacity values

Geocell reinforcement leads to benefits such as lower settlement and higher ultimate bearing capacity in different soil-supported structures, such as foundations. The extent of this improvement that geocell provides for the soil can be quantified by the Bearing Capacity Ratio (BCR), defined as the ratio of the bearing capacity in the reinforced condition to that in the unreinforced condition. The bearing capacities of 1574 unreinforced and reinforced samples were extracted from the stress-settlement curves, and Fig. 10 shows the distribution of the BCR values for the different soil samples.

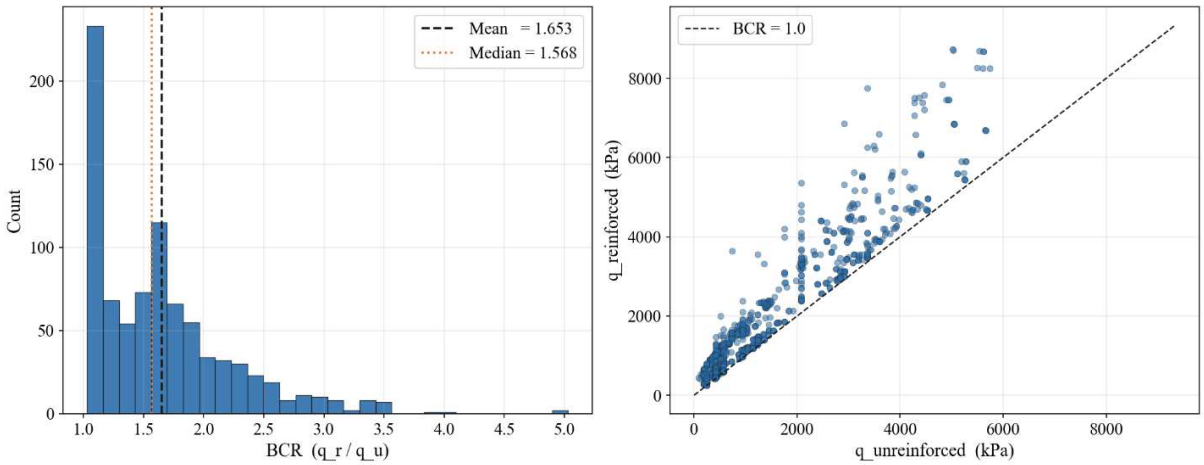

Fig. 10 Distribution of BCR values

The BCR values ranged approximately from 1 to 5, with an average value of 1.65. Most BCR values obtained from the simulations were larger than one, confirming the positive effect of geocell

reinforcement on foundation performance. The greater improvements are observed over weaker soil samples, whereas the provided lateral confinement by the geocell has led to a significant increase in the bearing capacities.

3.2 ANN Development and Performance

3.2.1 BC Model

The performance of the neural network was evaluated in this section using several metrics. In addition to the coefficient of determination (R^2), Root Mean Square Error (RMSE), and Mean Absolute Error (MAE), two specific indicators were used in this study: Nash–Sutcliffe model efficiency coefficient (NSE) and Mean Arctangent Absolute Percentage Error (MAAPE), whose formulations are summarized in Table 9. For single-output prediction problems, the mathematical formula of NSE and R^2 are equivalent; however, both metrics are reported as NSE is commonly used in geotechnical engineering studies. The average values of all metrics across the three runs are listed in Table 10. The R^2 values indicate that the model fits the data with high accuracy, whereas RMSE and MAE quantify the prediction errors in kPa. Given that the measured bearing capacity values ranged from 88 to 8729 kPa across both datasets, the obtained RMSE and MAE values represent only a small fraction of this range and therefore indicate satisfactory predictive performance. The high NSE values further confirm the strong predictive skill of the model. The predicted Bearing Capacity (BC) values are in good agreement with the numerical results obtained from the ABAQUS analysis. A slight decrease in prediction accuracy was observed for the reinforced dataset compared with the unreinforced dataset, which is expected because the reinforced model includes additional geocell-related input variables and thus makes the problem more complex and nonlinear.

Table 9 Mathematical formulation of the evaluation metrics

Metric	Formulation
R^2	$1-\frac{\sum(y_i-\hat{y}_i)^2}{\sum(y_i-\bar{y}_i)^2}$
RMSE	$\sqrt{\frac{1}{n}\sum(y_i-\hat{y}_i)^2}$
MAE	$\frac{1}{n}\lvert y_i-\hat{y}_i\rvert$
NSE	$1-\frac{\sum(y_i-\hat{y}_i)^2}{\sum(y_i-\bar{y}_i)^2}$
MAAPE	$\frac{1}{n}\sum\tan^{-1}\left(\frac{\lvert y_i-\hat{y}_i\rvert}{\lvert y_i\rvert}\right)$

Table 10 Average ANN performance metrics for the bearing capacity (BC) model

Dataset	RMSE	MAE	R^2	NSE	MAAPE
Unreinforced	183.19	130.65	0.986	0.986	0.100
Reinforced	391.55	248.57	0.914	0.914	0.185

Fig. 11 compares the model predictions with the corresponding values from the numerical simulations for the independent testing dataset. Most predictions are concentrated around the 1:1 line, indicating good agreement between the measured and predicted values. Moreover, many samples fall within the ±10% error bands, indicating the robustness of the model in capturing the nonlinear relationships between the input parameters. In addition to dividing the datasets into training, validation, and test subsets, a 5-fold cross-validation procedure was performed to further assess the robustness and generalization capability of the model. The average performance metrics obtained from the cross-validation analysis are presented in Table 11. The close agreement between the independent test metrics confirms that the model generalizes well without significant overfitting.

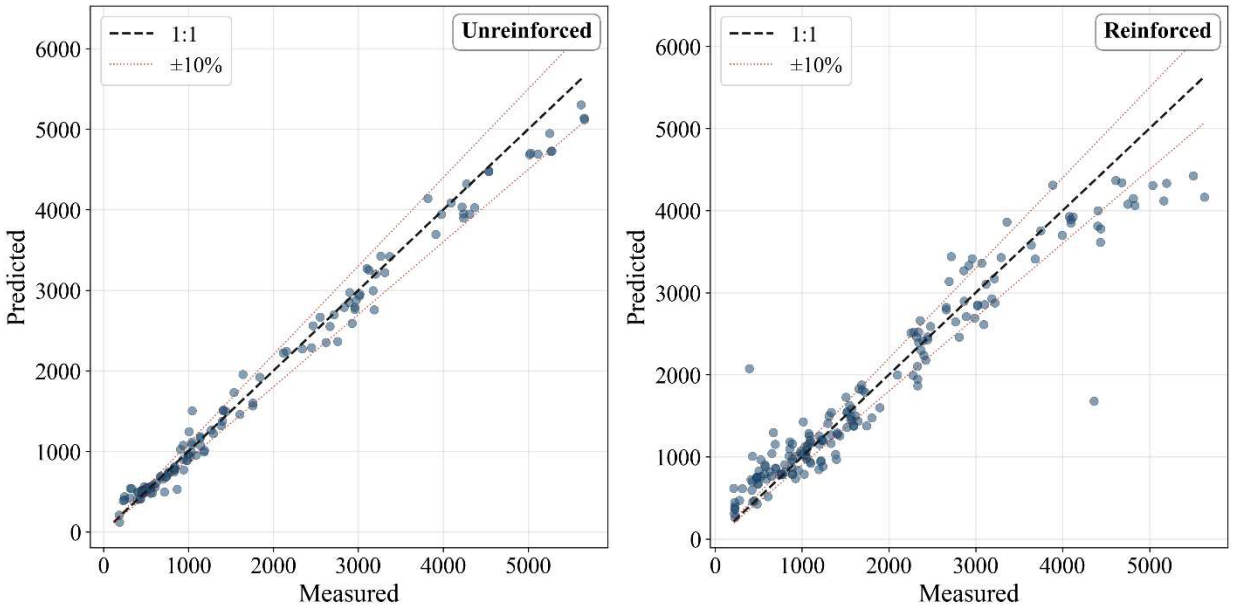

Fig. 11 Comparison of measured vs predicted bearing capacity values

Table 11 Average cross-validation metrics

Dataset	RMSE	MAE	R^2
Unreinforced	347.14	247.59	0.941
Reinforced	442.20	297.32	0.887

From an engineering perspective, the proposed model enables rapid prediction of the bearing capacity of a reinforced foundation without the need for multiple time-consuming FEM analyses. Once trained, the model can estimate the foundation response immediately, using basic soil and reinforcement parameters. This capability is particularly useful during the preliminary stages of design, as well as in sensitivity analyses and parametric studies, where a large number of simulations would otherwise be required.

3.2.2 BCR Model

The same metrics and visualizations were used for the bearing capacity ratio (BCR)model, where the target variable is the reinforcement benefit itself. The average performance metrics across five independent runs are reported in Table 12. Given that the mean BCR value in the dataset is 1.65 (as discussed in Section 3.1), the obtained RMSE and MAE values correspond to approximately 7–11% of this mean, indicating high predictive accuracy. Compared to the absolute bearing capacity (BC), BCR is a narrower and computationally more challenging target because it isolates the reinforcement effect from the dominant baseline contribution of the soil. Consequently, the achieved R^2 value of 0.883 represents a strong performance for reinforcement benefit prediction. The low per-seed variability of R^2 (± 0.004), combined with the close agreement between the cross-validation and test metrics, demonstrates the stability of the model and the absence of overfitting.

Fig. 12 compares the predicted and actual BCR values against the 1:1 line, and Fig. 13 shows the residual values of BCR across the range of values. The predicted BCR values are close to the 1:1 line, with most data points falling within the ±10% error bands. The residuals are randomly distributed around zero with no apparent systematic trend across the prediction range, indicating that the model is unbiased. The majority of residuals lie within ±0.3 BCR units and within the ±2σ (standard deviation) confidence bounds. The slight increase in scatter observed at higher BCR values reflects the right-skewed distribution of the target variable and the relatively sparser sampling of high-performance configurations. However, the implementation of the logarithmic transformation successfully mitigated most of this heteroscedasticity.

Table 12 Average ANN performance metrics for the BCR model

RMSE	MAE	R^2	NSE	MAAPE
0.185	0.128	0.883	0.883	0.076

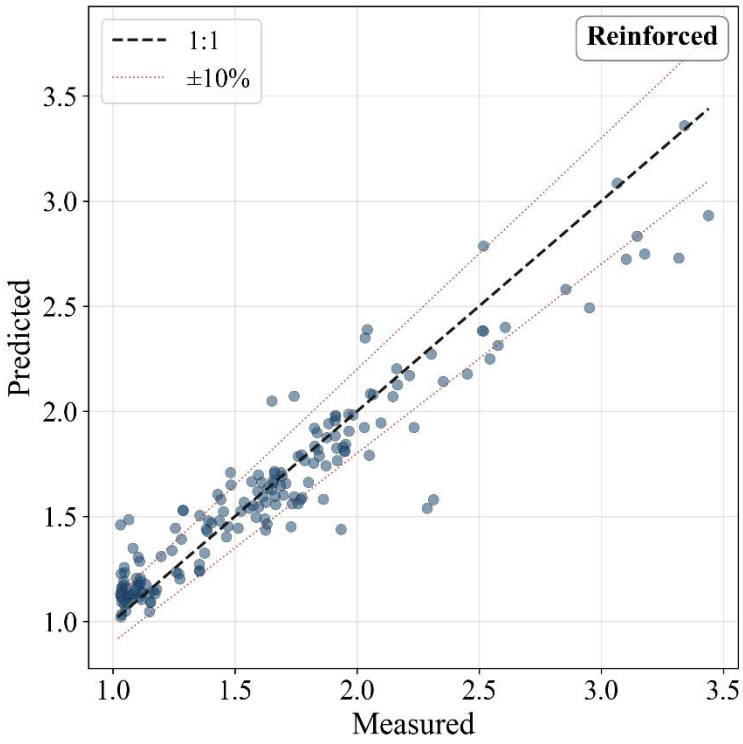

Fig. 12 Comparison of measured and predicted BCR values

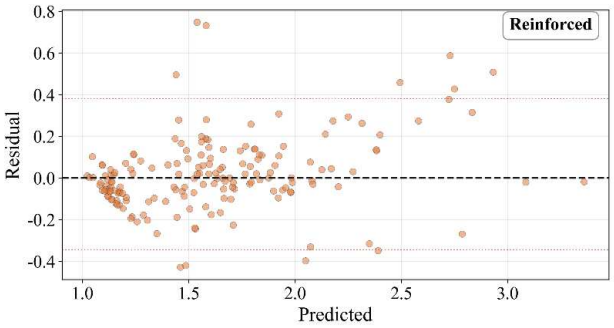

Fig. 13 Distribution of BCR residuals across the range of predicted values

The two models play complementary roles in this study. The BC model predicts absolute bearing capacity with high accuracy and serves as a rapid design-estimation tool, whereas the BCR model, despite its inherently lower R^2, targets a more complex parameter by isolating the reinforcement benefit, which is typically masked by the soil-dominated baseline in absolute capacity predictions. The negligible variability across random seeds (±0.004), together with the close agreement between cross-validation and test metrics confirms a stable, well-generalized model. Ultimately, this dual-modelling approach enables both accurate capacity prediction and a clear attribution of the factors governing reinforcement effectiveness, as analyzed in the subsequent section.

3.3 Model Interpretation

3.3.1 BC Model

As mentioned in the methodology, ANNs should be complemented with different tools to make the influence of individual input parameters on the prediction process observable. In the current study, Shapley Additive exPlanations (SHAP) were used to measure the impact of each feature on the predicted bearing capacity values and to increase the interpretability of the developed ANN model for bearing capacity. The average SHAP feature importance values for all input variables in each dataset are shown in Fig. 14. For the unreinforced dataset, soil cohesion, friction angle, and elastic modulus exhibited the highest SHAP values, indicating that soil stiffness and shear strength govern the foundation response. This, as the cohesion directly increases shear resistance, the friction angle governs confinement, and the elastic modulus controls stiffness and settlement. In the reinforced samples, the ratio of geocell layer width to foundation width and the foundation area were the most important parameters after the three primary soil strength features.

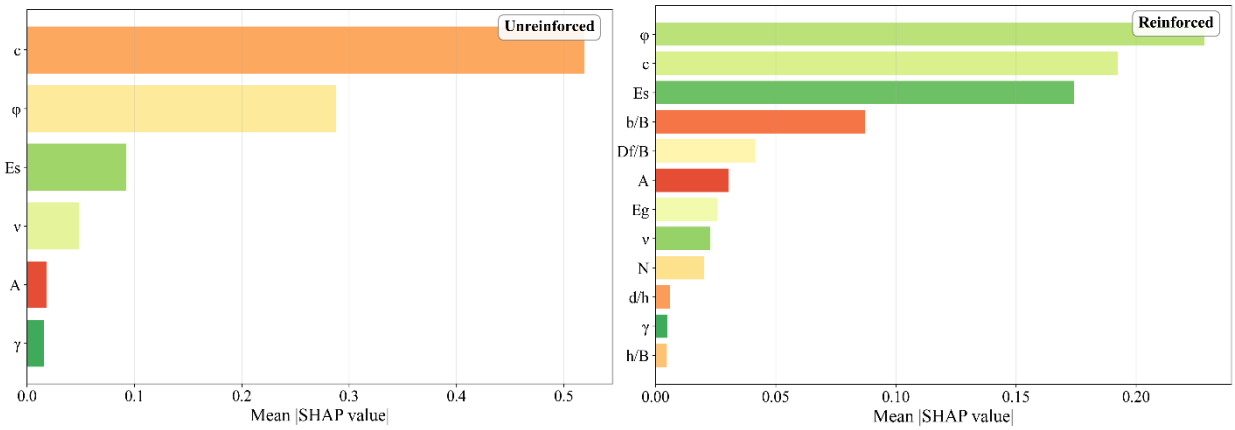

Fig. 14 Mean SHAP feature importance values for BC model

The SHAP summary plot, as shown in Fig. 15, illustrates both the magnitude and direction of the influence of each parameter. These plots illustrate the effect of a change in a specific input variable on the predicted output while accounting for interactions with other variables. SHAP importance values were also used to conduct a feature elimination process. To identify redundant input variables, the least influential parameter was eliminated in each iteration, the network was retrained, and the resulting change in performance was used to assess redundancy. This method confirmed that all retained inputs contributed non-redundantly to the prediction. For both datasets, cohesion was the most influential parameter affecting the predicted responses. In the reinforced dataset, cohesion was followed by the soil's friction angle and modulus. Together, these three features together accounted for most of the model response, indicating that soil strength parameters

govern the bearing behavior of geocell-reinforced foundations. The same pattern was observed in the unreinforced dataset, indicating that ANN correctly captures the fundamental geotechnical mechanisms. For the prediction of absolute bearing capacity, soil strength parameters such as c, φ, and Es dominate the response, since competent soil can sustain higher load with or without reinforcement. The geocell parameters exert a secondary influence on absolute capacity; their role in the reinforcement benefit is examined separately through the BCR model.

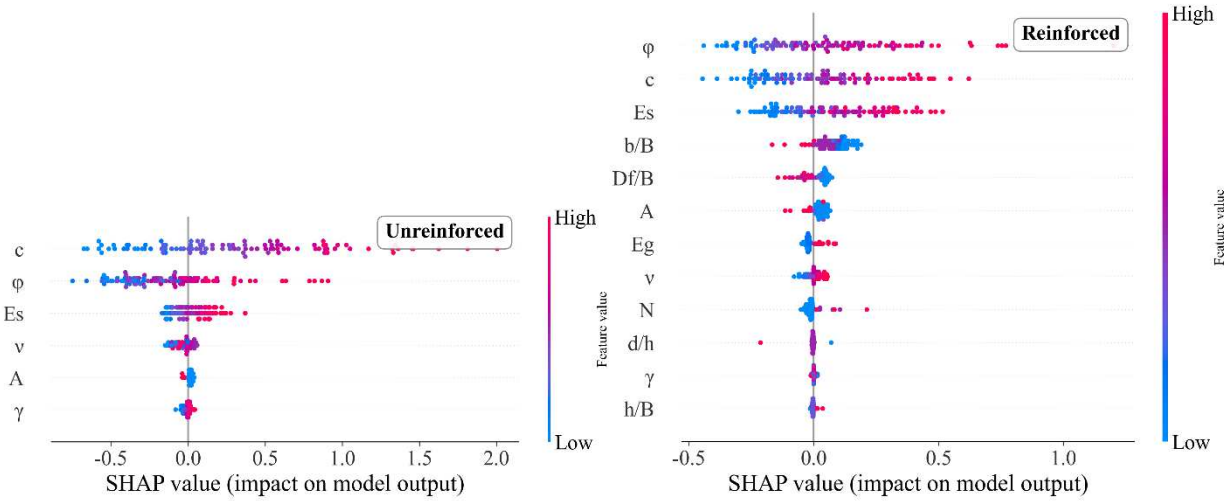

Fig. 15 SHAP summary for BC model

Partial dependence plots (PDPs) were generated for the most influential parameters in both datasets. PDP analysis was then used visualize the nonlinear relationships between the input features and the predicted output by showing the average effect of a single parameter on the outcome while averaging out the influence of all remaining variables. For the most important input variables, Figs. 16–18 show a rapid increase in the predicted bearing capacity while increasing parameter values in both datasets. In the unreinforced condition increases in cohesion and elastic modulus increase the bearing capacity up to a limiting value, while in the reinforced condition, the increase is more gradual and smoother.

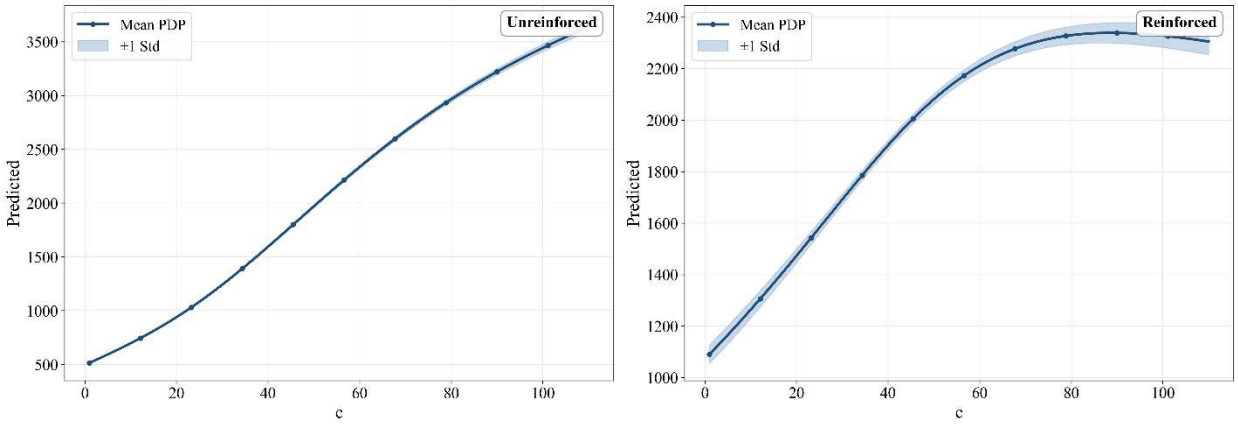

Fig. 16 Partial dependence plots of soil cohesion for BC model

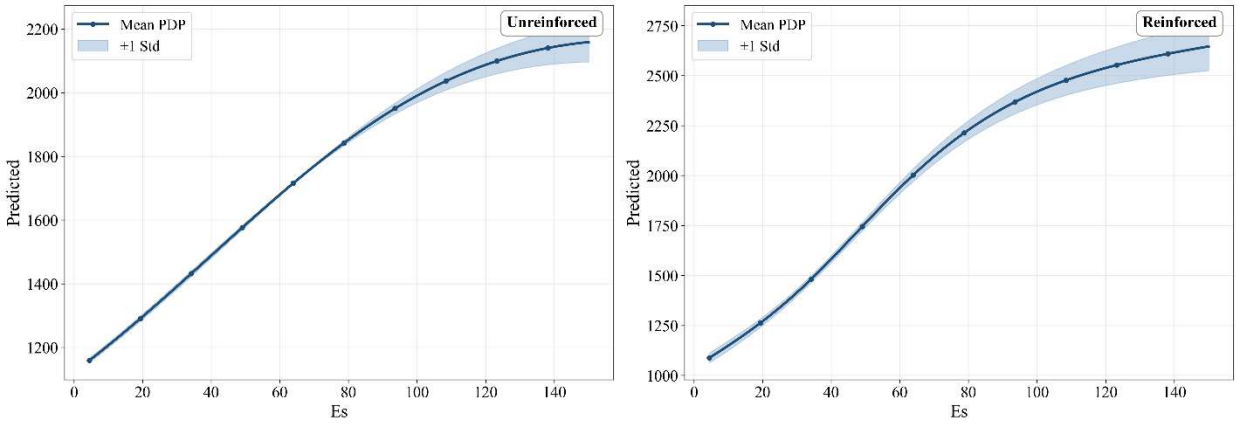

Fig. 17 Partial dependence plots of soil elastic modulus for BC model

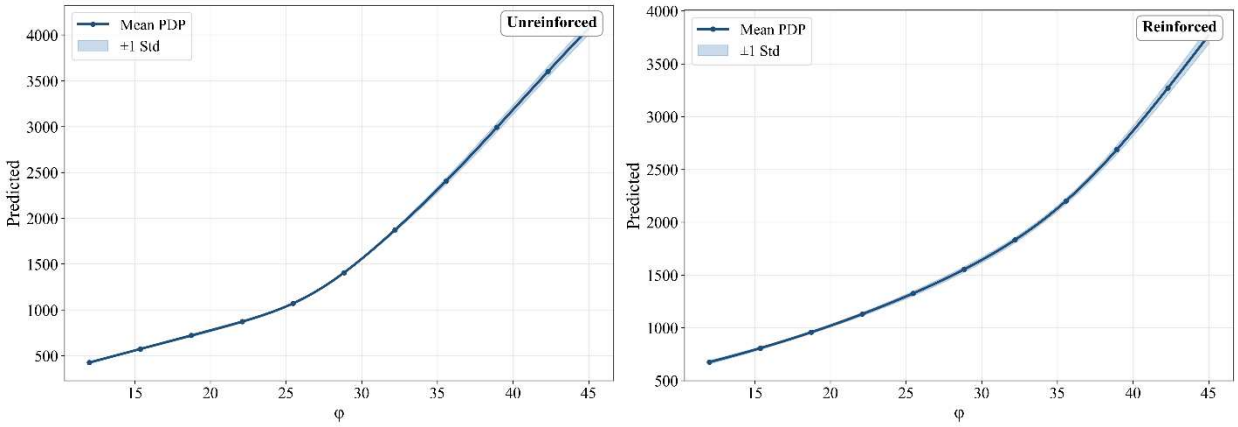

Fig. 18 Partial dependence plots of soil friction angle for BC model

3.3.2 BCR Model

Different interpretation tools were also used to reflect the results of the BCR model. Fig. 19 presents mean SHAP values for the different parameters. Elastic modulus of the geocell has the highest effect on the BCR, followed by embedment depth ratio and geocell layer width ratio.

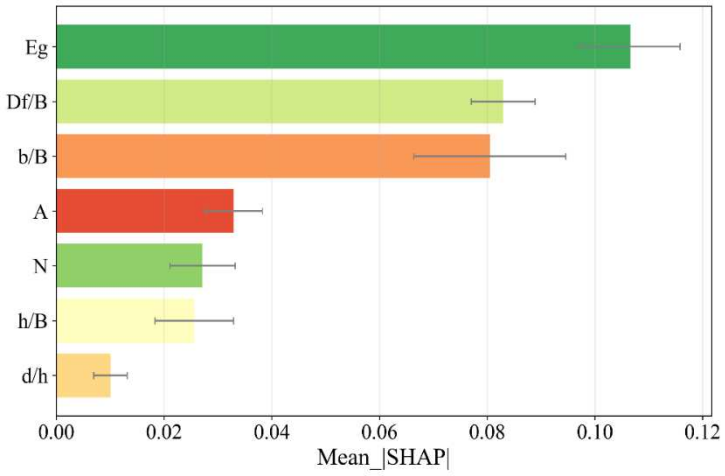

Fig. 19 Raw SHAP values for BCR model

A SHAP-guided backward feature elimination process was conducted for the BCR model. This analysis confirmed that the geocell variables carry genuine, non-redundant signal, and removing geocell parameters like b/B, Eg, and Df/B sharply reduced the BCR R^2, whereas the full 12-feature model retained the best performance.

The partial-dependence plots clarify the direction of each parameter's effect. Fig. 20 shows partial dependence plots for the some geocell-related parameters in the BCR model: (a) geocell modulus, Eg; (b) height ratio, h/B; (c) embedment-depth ratio, Df/B; and (d) pocket aspect ratio, d/h. BCR increases markedly with geocell modulus and height ratio (h/B), confirming that a stiffer and higher geocell mobilizes greater lateral confinement and thus larger reinforcement benefit, Conversely, the BCR decreases with increasing d/h and Df/B, indicating that smaller geocell openings and lower embedment depths can result in a higher BCR.

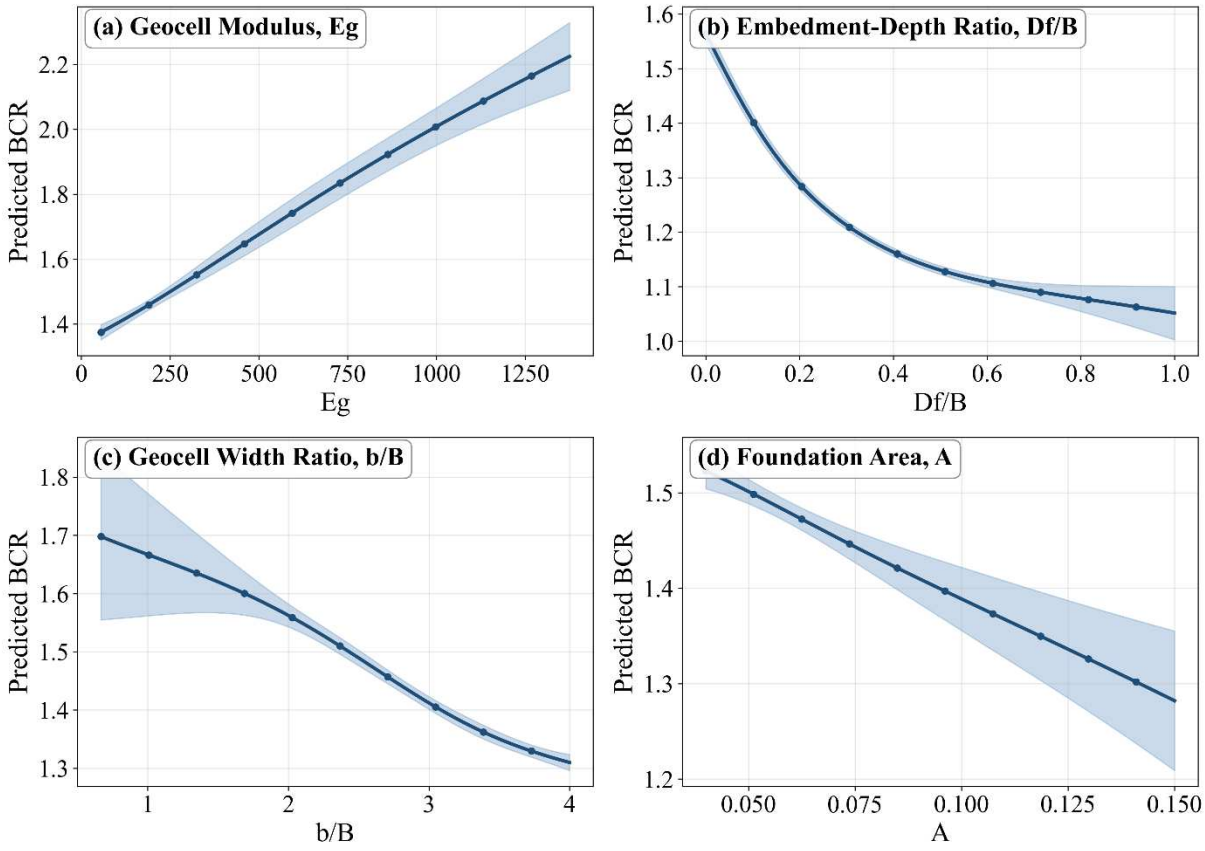

Fig. 20 Partial dependence plots of the most influential parameters in the BCR model

4. Conclusions

This study developed an Artificial Neural Networks (ANNs) framework for predicting the bearing capacity of unreinforced and geocell-reinforced foundations and for quantifying the associated reinforcement benefit. To this aim, at first, a three-dimensional finite-element model was established in ABAQUS and validated against the experimental results reported by Hegde and Sitharam (2015). A comprehensive numerical database was subsequently generated by varying soil, footing, and geocell properties. The resulting dataset was the used to develop separate ANN models for both the bearing capacity (BC) and bearing-capacity ratio (BCR), while SHAP analysis, SHAP-guided feature elimination, and partial dependence plots (PDPs) were employed to interpret the models and identify the governing parameters. The principal findings are summarized as follows:

- A comprehensive and thorough database of 1574 foundation analyses was developed by considering a wide range of soil properties, geocell parameters, and foundation dimensions. The outcome was stress-settlement curves for each sample covering a wide range of

foundation behaviors. the results demonstrated the capabilities ANN in accurately representing different types of reinforced foundation systems.

- Geocell reinforcement considerably improved the bearing capacity and ultimate stress of the foundation beds. The simulations in this study involved a vast range of BCR values from approximately 1 to 5, with an average value of 1.65, indicating that the efficiency of geocell reinforcement is highly dependent on soil and reinforcement characteristics.
- The developed ANN models successfully captured the nonlinear relationships between the input parameters and foundation response. The BC model achieved average coefficients of determination of R^2=0.914 and R^2=0.986 for reinforced model and unreinforced conditions, respectively, indicating high prediction accuracy and relatively low errors. The independent BCR model achieved an R^2 of 0.883, demonstrating reliable prediction of the relatively more complex reinforcement-effectiveness indicator.
- Comparison of the ANN predictions with the results of the validated numerical model showed close agreement. Most predicted values exhibited low residuals and fell within the ±10% error bounds. therefore, the proposed ANN models can reproduce the finite-element results with satisfactory accuracy while requiring substantially lower computational time and effort than repeated three-dimensional numerical analyses.
- SHAP-based interpretation showed that soil cohesion (c), friction angle (φ), and elastic modulus (E_s) were the dominant parameters governing the bearing capacity of the foundation since soil shear strength and stiffness primarily control the load-carrying capacity of shallow foundations, irrespective of the presence of reinforcement.
- The complementary BCR model demonstrated greater improvement in weaker soils. Among the geocell-related variables, the stiffness (E_g), geocell embedment ratio (D_f/B), and geocell width ratio (b/B) were confirmed by feature-elimination to contribute a genuine, non-redundant predictive signal.
- The proposed ANN models provide a useful and efficient alternative to repeated FEM analyses for predicting the behavior of geocell-reinforced foundation beds. Owing to their computational efficiency, the developed models can be used as predictive tools for reinforcement designs and related parametric investigations.

5. Statements & Declarations

Author contributions

Mohammad Javad Hosseinzadeh: Investigation, Formal analysis, Data curation, Software, Writing - Original Draft.

Mohammad Oliaei: Conceptualization, Supervision, Project administration, Resources.

Saeed Kouzegaran: Writing - Review & Editing, Supervision.

Funding

The authors received no financial support for the research, authorship, and/or publication of this article.

Declarations

The authors declare no conflict of interest.

6. References

1 Guido, V. A., Chang, D. K. & Sweeney, M. A. Comparison of geogrid and geotextile reinforced earth slabs. *Canadian Geotechnical Journal* **23**, 435–440 (1986).

2 Abu-Farsakh, M., Chen, Q. & Sharma, R. An experimental evaluation of the behavior of footings on geosynthetic-reinforced sand. *Soils and Foundations* **53**, 335–348 (2013).

3 Chen, J. *et al.* Physical and numerical modelling of strip footing on geogrid reinforced transparent sand. *Geotextiles and Geomembranes* **49**, 399–412 (2021).

4 Latha, G. M. & Murthy, V. S. Effects of reinforcement form on the behavior of geosynthetic reinforced sand. *Geotextiles and Geomembranes* **25**, 23–32 (2007).

5 Pordel, M. & Kouzegaran, S. A Comparative Study on the Mechanical Performance of Unreinforced and Reinforced Stone Columns Using Geotextile and Recycled Tire Crumbs. (2025).

6 Wang, J.-Q., Zhang, L.-L., Xue, J.-F. & Tang, Y. Load-settlement response of shallow square footings on geogrid-reinforced sand under cyclic loading. *Geotextiles and Geomembranes* **46**, 586–596 (2018).

7 Xu, C., Liang, C. & Shen, P. Experimental and theoretical studies on the ultimate bearing capacity of geogrid-reinforced sand. *Geotextiles and Geomembranes* **47**, 417–428 (2019).

8 Chen, Q. & Abu-Farsakh, M. Ultimate bearing capacity analysis of strip footings on reinforced soil foundation. *Soils and Foundations* **55**, 74–85 (2015).

9 Huang, C.-C. & Tatsuoka, F. Bearing capacity of reinforced horizontal sandy ground. *Geotextiles and Geomembranes* **9**, 51–82 (1990).

10 Huang, C.-C. Settlement of footings on reinforced level sandy ground at peak footing loads. *Geosynthetics International* **18**, 124–136 (2011).

11 Raja, M. N. A. & Shukla, S. K. Ultimate bearing capacity of strip footing resting on soil bed strengthened by wraparound geosynthetic reinforcement technique. *Geotextiles and Geomembranes* **48**, 867–874 (2020).

12 Oliaei, M. & Kouzegaran, S. Efficiency of cellular geosynthetics for foundation reinforcement. *Geotextiles and Geomembranes* **45**, 11–22 (2017).

13 Tafreshi, S. M. & Dawson, A. R. Comparison of bearing capacity of a strip footing on sand with geocell and with planar forms of geotextile reinforcement. *Geotextiles and Geomembranes* **28**, 72–84 (2010).

14 Dash, S., Rajagopal, K. & Krishnaswamy, N. Performance of different geosynthetic reinforcement materials in sand foundations. *Geosynthetics International* **11**, 35–42 (2004).

15 Kouzegaran, S. & Oliaei, M. Numerical analysis of the cellular geosynthetics performance in unpaved roads and influencing factors. *Transportation Infrastructure Geotechnology* **12**, 108 (2025).

16 Nazzal, M. D., Abu-Farsakh, M. Y. & Mohammad, L. N. Implementation of a critical state two-surface model to evaluate the response of geosynthetic reinforced pavements. *International Journal of Geomechanics* **10**, 202–212 (2010).

17 Zhang, L., Zhao, M., Shi, C. & Zhao, H. Bearing capacity of geocell reinforcement in embankment engineering. *Geotextiles and Geomembranes* **28**, 475–482 (2010).

18 Dash, S. K., Sireesh, S. & Sitharam, T. Model studies on circular footing supported on geocell reinforced sand underlain by soft clay. *Geotextiles and Geomembranes* **21**, 197–219 (2003).

19 Sireesh, S., Sitharam, T. & Dash, S. K. Bearing capacity of circular footing on geocell–sand mattress overlying clay bed with void. *Geotextiles and Geomembranes* **27**, 89–98 (2009).
20 Satyal, S. R., Leshchinsky, B., Han, J. & Neupane, M. Use of cellular confinement for improved railway performance on soft subgrades. *Geotextiles and Geomembranes* **46**, 190–205 (2018).
21 Han, J., Yang, X., Leshchinsky, D. & Parsons, R. L. Behavior of geocell-reinforced sand under a vertical load. *Transportation Research Record* **2045**, 95–101 (2008).
22 Talebi, M., Oliaei, M. & Kouzegaran, S. Numerical Investigation of Uplift Capacity Enhancement of Horizontal Plate Anchors Using Geocell Reinforcement. *Civil Engineering and Applied Solutions* **20**, XX–XX (2026).
23 Dash, S. K. & Choudhary, A. K. Geocell reinforcement for performance improvement of vertical plate anchors in sand. *Geotextiles and Geomembranes* **46**, 214–225 (2018).
24 Chen, R.-H., Huang, Y.-W. & Huang, F.-C. Confinement effect of geocells on sand samples under triaxial compression. *Geotextiles and Geomembranes* **37**, 35–44 (2013).
25 Pokharel, S. K., Han, J., Leshchinsky, D., Parsons, R. L. & Halahmi, I. Investigation of factors influencing behavior of single geocell-reinforced bases under static loading. *Geotextiles and Geomembranes* **28**, 570–578 (2010).
26 Song, F., Liu, H., Yang, B. & Zhao, J. Large-scale triaxial compression tests of geocell-reinforced sand. *Geosynthetics International* **26**, 388–395 (2019).
27 Zhang, M., Javadi, A. & Min, X. Triaxial tests of sand reinforced with 3D inclusions. *Geotextiles and Geomembranes* **24**, 201–209 (2006).
28 Mani, G., Subramanian, S. & Jagadesh, P. Bearing capacity and settlement behavior of square footing on coir geocell–reinforced sand under concentric and eccentric loading. *Scientific Reports* (2026).
29 Saride, S., Gowrisetti, S., Sitharam, T. & Puppala, A. J. Numerical simulation of geocell-reinforced sand and clay. *Proceedings of the institution of civil engineers-ground improvement* **162**, 185–198 (2009).
30 Hegde, A. & Sitharam, T. 3-Dimensional numerical modelling of geocell reinforced sand beds. *Geotextiles and Geomembranes* **43**, 171–181 (2015).
31 Zhao, Y., Lu, Z., Liu, J., Zhang, J. & Yao, H. Influence of different infill materials on the performance of geocell-reinforced cohesive soil beds. *Scientific Reports* **13**, 12330 (2023).
32 Hosseinzadeh, M. J. & Oliaei, M. Numerical Analysis of Geocell-Reinforced Foundations under Varying Soil Conditions. *Civil Engineering and Applied Solutions* **2**, 69–78 (2026).
33 Latha, G. M., Dash, S. K. & Rajagopal, K. Numerical simulation of the behavior of geocell reinforced sand in foundations. *International Journal of Geomechanics* **9**, 143–152 (2009).
34 Mehdipour, I., Ghazavi, M. & Moayed, R. Z. Numerical study on stability analysis of geocell reinforced slopes by considering the bending effect. *Geotextiles and Geomembranes* **37**, 23–34 (2013).
35 Sitharam, T. & Hegde, A. Design and construction of geocell foundation to support the embankment on settled red mud. *Geotextiles and Geomembranes* **41**, 55–63 (2013).
36 Zhou, H. & Wen, X. Model studies on geogrid-or geocell-reinforced sand cushion on soft soil. *Geotextiles and Geomembranes* **26**, 231–238 (2008).
37 Liu, Y. & Liang, Y. Integrated machine learning for modeling bearing capacity of shallow foundations. *Scientific Reports* **14**, 8319 (2024).

38 Shah, J., Alam, M., Javed, F., Umar, M. & Ahmad, F. Comparative performance evaluation of machine learning models for predicting the ultimate bearing capacity of shallow foundations on granular soils. *Scientific Reports* **15**, 36525 (2025).
39 Raja, M. N. A. & Shukla, S. K. Predicting the settlement of geosynthetic-reinforced soil foundations using evolutionary artificial intelligence technique. *Geotextiles and Geomembranes* **49**, 1280–1293 (2021).
40 Raja, M. N. A., Jaffar, S. T. A., Bardhan, A. & Shukla, S. K. Predicting and validating the load-settlement behavior of large-scale geosynthetic-reinforced soil abutments using hybrid intelligent modeling. *Journal of Rock Mechanics and Geotechnical Engineering* **15**, 773–788 (2023).
41 Kumar, V., Priyadarshee, A., Chandra, S., Jindal, A. & Rana, D. Behavioral study of raft reinforced with geogrid and geocell through experiments and neural models. *Civil Engineering Infrastructures Journal* **56**, 321–332 (2023).
42 Saride, S., Sitharam, T. & Puppala, A. J. in *Ground Improvement and Geosynthetics* 328–337 (2010).
43 Kumar, V. & Kumar, A. Predicting the settlement of raft resting on sand reinforced with planar and geocell using generalized regression neural networks (GRNN) and back propagated neural networks (BPNN). *International Journal of Geosynthetics and Ground Engineering* **4**, 30 (2018).
44 Trujillo, H., Avesani Neto, J. & Zornberg, J. Integrating supervised machine learning with laboratory data to evaluate the modulus improvement factor in geocell-reinforced soils. *International Journal of Geosynthetics and Ground Engineering* **11**, 69 (2025).
45 Venkateswarlu, H., Sharma, S. & Hegde, A. Performance of genetic programming and multivariate adaptive regression spline models to predict vibration response of geocell reinforced soil bed: a comparative study. *International Journal of Geosynthetics and Ground Engineering* **7**, 63 (2021).
46 Feng, Y., Bo, Y. & Chen, Z. Bearing performance and failure-mode prediction of geocell-reinforced foundations. *Scientific Reports* (2026).
47 Goh, A. Empirical design in geotechnics using neural networks. *Geotechnique* **45**, 709–714 (1995).
48 Bowles, J. E. *Physical and geotechnical properties of soils*. (1981).
49 Bowles, J. E. & Guo, Y. *Foundation analysis and design*. Vol. 5 (McGraw-hill, New York, 1996).
50 Coduto, D. P. *Foundation design: principles and practices*. (Pearson, 2015).
51 Coduto, D. P., Yeung, M.-c. R. & Kitch, W. A. Geotechnical engineering: principles and practices. (2011).
52 Das, B. M. & Sobhan, K. Principles of geotechnical engineering. (2006).
53 Murthy, V. *Geotechnical engineering: principles and practices of soil mechanics and foundation engineering*. (CRC press ---, 2019).
54 Obrzud, R. *The hardening soil model: A practical guidebook*. (Zace Services ---, 2010).
55 Jain, A., Punmia, B. & Jain, E. Soil mechanics and foundations. *Firewall Media*, 111–129 (2005).
56 Terzaghi, K., Peck, R. B. & Mesri, G. Soil mechanics in engineering practice. (1996).
57 Myers, J. L., Well, A. D. & Lorch Jr, R. F. *Research design and statistical analysis*. (Routledge ---, 2013).